AD-A138 633 F-LAYER IONIZATION PATCHES IN THE POLAR CAP(U) AIR FORCE GEOPHYSICS LAB HANSCOM AFB MA E J WEBER ET AL. 05 OCT 83 AFGL-TR-83-0276 1/

UNCLASSIFIED F/G 4/1 NL

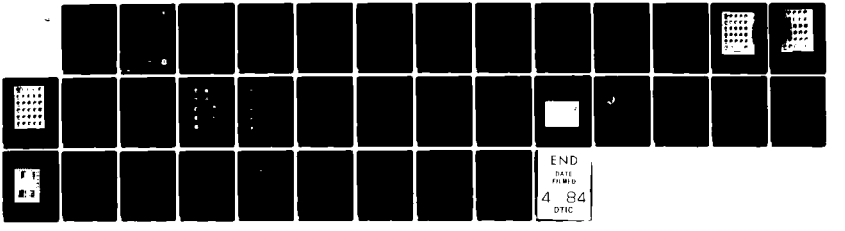

END
DATE FILMED
4 84
DTIC

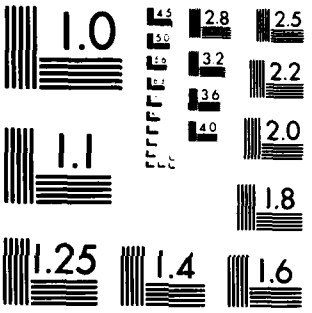

MICROCOPY RESOLUTION TEST CHART
NATIONAL BUREAU OF STANDARDS 1963-A

AFGL-TR-83-0276
ENVIRONMENTAL RESEARCH PAPERS, NO. 888

(12)

F-Layer Ionization Patches in the Polar Cap

E. J. WEBER
J. BUCHAU
J. G. MOORE
J. R. SHARBER
R. C. LIVINGSTON
J. D. WINNINGHAM
B. W. REINISCH

5 October 1983

SPACE PHYSICS DIVISION PROJECT 4643
AIR FORCE GEOPHYSICS LABORATORY
HANSCOM AFB, MASSACHUSETTS 01731

AIR FORCE SYSTEMS COMMAND, USAF

This report has been reviewed by the ESD Public Affairs (PA) and is releasable to the National Technical Information Service (NTIS)

"This technical report has been reviewed and is approved for publication"

FOR THE COMMANDER

for HERBERT C. CARLSON
Branch Chief

RITA C. SAGALYN
Division Director

Qualified requestors may obtain additional copies from the Defense Technical Information Center. All others should apply to the National Technical Information Service.

If your address has changed, or if you wish to be removed from the mailing list, or if the addressee is no longer employed by your organization, please notify AFGL/DAA, Hanscom AFB, MA 01731. This will assist us in maintaining a current mailing list.

Do not return copies of this report unless contractual obligations or notices on a specific document requires that it be returned.

Unclassified

SECURITY CLASSIFICATION OF THIS PAGE (When Data Entered)

REPORT DOCUMENTATION PAGE	READ INSTRUCTIONS BEFORE COMPLETING FORM
1. REPORT NUMBER AFGL-TR-83-0276	2. GOVT ACCESSION NO AD-A138633
3. RECIPIENT'S CATALOG NUMBER	
4. TITLE (and Subtitle) F-LAYER IONIZATION PATCHES IN THE POLAR CAP	5. TYPE OF REPORT & PERIOD COVERED Scientific. Interim.
6. PERFORMING ORG. REPORT NUMBER ERP No. 859	
7. AUTHOR(s) E. J. Weber J. R. Sharber* B. W. Reinisch†† J. Buchau R. C. Livingston** J. G. Moore J. D. Winningham†	8. CONTRACT OR GRANT NUMBER(s)
9. PERFORMING ORGANIZATION NAME AND ADDRESS Air Force Geophysics Laboratory (PHY) Hanscom AFB Massachusetts 01731	10. PROGRAM ELEMENT, PROJECT, TASK AREA & WORK UNIT NUMBERS 62101F 46430801
11. CONTROLLING OFFICE NAME AND ADDRESS Air Force Geophysics Laboratory (PHY) Hanscom AFB Massachusetts 01731	12. REPORT DATE 5 October 1983 13. NUMBER OF PAGES 34
14. MONITORING AGENCY NAME & ADDRESS(if different from Controlling Office)	15. SECURITY CLASS. (of this report) Unclassified 15a. DECLASSIFICATION DOWNGRADING SCHEDULE

16. DISTRIBUTION STATEMENT (of this Report)

Approved for public release; distribution unlimited

17. DISTRIBUTION STATEMENT (of the abstract entered in Block 20, if different from Report)

18. SUPPLEMENTARY NOTES

*Physics and Space Sci. Dept., Florida Inst. of Tech., Melbourne, FL 32901
**Radio Physics Lab, SRI Int'l, Menlo Park, CA 94025
†Southwest Research Inst., San Antonio, TX 78284
††University of Lowell, Center for Atmospheric Research

19. KEY WORDS (Continue on reverse side if necessary and identify by block number)

Polar F-Layer
Convection
Scintillation

20. ABSTRACT (Continue on reverse side if necessary and identify by block number)

Ground based optical and digital ionosonde measurements were conducted at Thule, Greenland, to measure ionospheric structure and dynamics in the nighttime polar cap F-layer. These observations showed the existence of large scale (800—1000 km) plasma patches drifting in the anti-sunward direction during a moderately disturbed ($K_p > 4$) period. Simultaneous Dynamics Explorer (DE—2) Low Altitude Plasma Instrument (LAPI) measurements show that these patches, with peak densities of $\sim 10^6$ el cm^{-3}, are not locally produced by structured particle precipitation. The LAPI measurements show

DD FORM 1 JAN 73 1473 EDITION OF 1 NOV 65 IS OBSOLETE

Unclassified

SECURITY CLASSIFICATION OF THIS PAGE (When Data Entered)

approx. = $1/cm^3$

20 (contd)

a uniform precipitation of polar-rain electrons over the polar cap. The combined measurements provide a comprehensive description of patch structure and dynamics. They are produced near or equatorward of the dayside auroral zone, and convect across the polar cap in the anti-sunward direction. As gradients within the large scale, drifting patches are subject to structuring by convective instabilities. The resulting irregularity distribution within the patches is mapped using uhf scintillation and spaced-receiver measurements.

Preface

The authors wish to thank R.W. Gowell, J.W.F. Lloyd, and J.B. Waarama of AFGL for engineering support; M. Shirley, University of Lowell, and W. Whiting, Regis College, for analysis support.

Assistance with the auroral ionization/emission code was generously provided by D. J. Strickland.

The support and cooperation of the flight crew and ground personnel of the 4950th TW, AFSC, Wright-Patterson AFB, Dayton, Ohio, is gratefully acknowledged.

This research was supported in part by the following contracts: DNA S99ZAXHC WU20/21 (AFGL), AFGL F19628-80-C-0064 (Univ. of Lowell), NASA NAS 5-26363 and AFGL FY712183N0001 (SWRI), and AFGL under Sandia 55-3136 (SRI).

Contents

1. INTRODUCTION 7

2. OBSERVATIONS 9

   2.1 Optical Measurements 9
   2.2 Ionosonde Measurements 14
   2.3 Precipitating Particle Characteristics 21
   2.4 Intermediate Scale Structure 27

3. CONCLUSIONS 31

REFERENCES 33

Illustrations

1a. Sequence of 6300 Å ASIP Images at 3-Min Intervals From 07:03 to 08:27 UT, 22 Jan 1982, From Thule, Greenland 10

1b. Sequence of 6300 Å ASIP Images at 3-Min Intervals From 08:33 09:57 UT, 22 Jan 1982, From Thule, Greenland 11

1c. Sequence of 6300 Å ASIP Images at 3-Min Intervals From 10:03 to 11:27 UT, 22 Jan 1982, From Thule, Greenland 12

2. 6300 Å Zenith Intensity From 06:30 to 11:35 UT, 22 Jan 1982 From Thule, Greenland 13

3. Sequence of 6300 Å ASIP Images From 10:06 to 10:41 UT, 22 Jan 1982, From Thule, Greenland 15

4. Sequence of 6300 Å ASIP Images From 10:46 to 11:11 UT, 22 Jan 1982, From Thule, Greenland 16

5. Electron Density Contours Along the Noon—Midnight Axis of the Ionization Patch Observed From 10:06 to 10:51 UT, 22 Jan 1982, From Thule, Greenland 19

6. Integrated Height Characteristic Using Both Positive- and Negative-Doppler Ionograms for 22 Jan 1982 20

7. Energy-Time Spectrogram on the 06:55 UT Pass of DE—2 Satellite Over the Northern Polar Cap on 22 Jan 1982 21

8. 6300 Å ASIP Image at 06:54 UT, 22 Jan 1982, From Thule, Greenland 22

9. Electron Sources of 6300 Å Emission and F-Layer Ionization Showing Polar Rain and Photoelectron Spectra During the 06:55 and 10:07 UT Passes 23

10. Electron Density Profiles Inside and Outside the F-Layer Patch Determined From True Height Analysis of Ionograms 25

11. Energy-Time Spectrogram on the 10:07 UT Pass of DE—2 Over the Northern Polar Cap on 22 Jan 1982 26

12. Intensity Scintillation Index and Turbulence Strength for 22 Jan 1982 28

13. CGL/Local Time Plot Showing Irregularity Drift Pattern Determined From Spaced-Receiver Scintillation Measurements 30

F-Layer Ionization Patches in the Polar Cap

1. INTRODUCTION

In addition to solar ionization, polar cap F-layer structure is controlled by direct precipitation of low energy electrons and by plasma convection. As outlined by Kelley et al,[1] these are also controlling factors for the generation, transport, and decay of ionospheric irregularities that exist over a wide range of scale sizes in the polar region.

Previous coordinated measurements in the polar cap[2] have shown the structure and drift of sub-visual F-layer auroras. They are noon-midnight aligned, drift predominantly in the dawn-to-dusk direction, and are produced by fluxes of low energy ($E < 500$ eV) electrons. Intense ionospheric irregularities within the auroral arcs cause amplitude and phase fluctuations, called scintillation, on satellite-to-ground uhf radio transmission, and spread F on the ionosonde hf echo returns.

In a recent study, Hardy[3] has classified types of electron fluxes precipitating

(Received for publication 5 October 1983)

1. Kelley, M.C., Vickrey, J.F., Carlson, C.W., and Torbert, R. (1982) On the origin and spatial extent of high-latitude F-region irregularities, J. Geophys. Res. 87:4469.

2. Weber, E.J., and Buchau, J. (1981) Polar cap F layer auroras, Geophys. Res. Lett. 8:125.

3. Hardy, D.A. (1983) Intense fluxes of low energy electrons above the auroral oval and in the polar cap, J. Geophys. Res. (in press).

into the polar cap. His Class III spectra (accelerated through a field-aligned potential gradient from 50 V to 2 kV) are most clearly associated with the observed ionospheric characteristics of the sub-visual F-layer arcs. They are the polar showers reported by Winningham and Heikkila.[4] An important result from Hardy's[3] satellite measurements is the strong dependence on the occurrence of electron fluxes in the polar cap with the north-south component of the interplanetary magnetic field (B_z). A positive correlation exists between the presence (absence) of accelerated electron fluxes above polar rain energy in the polar cap with northward (southward) B_z. The occurrence of more intense (visible) auroras, measured by all-sky cameras[5] and by the DMSP satellite imager,[6] also show a positive correlation with northward B_z. Thus, during times of northward B_z, and statistically during quiet geomagnetic conditions as measured by K_p and AE,[7] accelerated polar rain electrons (polar showers) precipitate into the polar cap and produce F-layer auroras and associated ionospheric irregularities. However, uhf scintillation measurements, a measure of km-scale irregularities, do not show a strong dependence on the level of geomagnetic activity. Scintillation occurrence measured from Thule, Greenland (86° CGL), was shown by Aarons et al[8] to be essentially independent of K_p. Thus, during disturbed geomagnetic periods, when structured particle precipitation into the polar cap does not directly produce the observed irregularities, transport of plasma and irregularities from other production regions must be considered.

The purpose of this paper is to describe large scale (~1000 km) plasma patches observed in the polar cap during a moderately disturbed ($K_p \geq 4$) period. The patches, observed by optical and radio techniques, are convected in the anti-sunward direction across the central polar cap from a source region near the dayside auroral oval. Spaced receiver and uhf scintillation measurements provide an estimate of irregularity intensity and drift velocity. Simultaneous Dynamics Explorer (DE—2) Low Altitude Plasma Instrument (LAPI) measurements show a uniform precipitation of polar rain; regions of accelerated and structured low-energy electron precipitation were not observed.

---

4. Winningham, J.D., and Heikkila, W.J. (1974) Polar cap auroral electron fluxes observed with ISIS I, J. Geophys. Res. 79:949.
5. Lassen, K., and Danielsen, C. (1978) Quiet time pattern of auroral arcs for different directions of the interplanetary magnetic field in the y-z plane, J. Geophys. Res. 83:5277.
6. Gussenhoven, M.S. (1982) Extremely high latitude auroras, J. Geophys. Res. 87:2401.
7. Maezawa, K. (1978) Dependence of geomagnetic activity on solar wind parameters: A statistical approach, Solar Terr. Environ. Res., Japan, 2:103.
8. Aarons, J., Mullen, J.P., Whitney, H.E., Johnson, A.L., and Weber, E.J. (1981) UHF scintillation over polar latitudes, Geophys. Res. Lett. 8:277.

Recently, Kelley et al[1] have incorporated many of the observed features of high latitude irregularities in a convection/decay model. The results of this study and those of Weber and Buchau[2] on direct irregularity production will improve irregularity source functions in future models.

2. OBSERVATIONS

Polar cap ionospheric measurements were conducted from Thule Air Base, Greenland (76.5° N, 68.7° W, 86° CGL), from 17 to 27 January 1982. The objectives of these experiments were to measure optical and radio-wave signatures of polar cap ionospheric structures, to relate these to in situ measurements from the DE—2 satellite, and to determine the relation of the large scale plasma structures to small scale (km) irregularities through satellite—ground scintillation measurements.

2.1 Optical Measurements

Optical measurements were performed using a wide angle (155° field of view) All-Sky Imaging Photometer (ASIP)[9] with interference filters to measure 6300 Å and 7774 Å OI, 4278 Å N_2^+, and 5200 Å NI. Figures 1a—1c show a sequence of 6300 Å ASIP images at 3-min intervals from 07:00 to 11:27 UT, 22 January 1982. The images were made using a 30-sec integration time, and they cover a dynamic range of ~20—400 Rayleighs (R). For an assumed emission height of 250 km, the total image diameter is ~1600 km (lens vignetting reduces the useful diameter to ~ 1200 km). For spatial reference, the dawn—dusk (06—18) and noon—midnight (12—00) CG meridians are projected into the images for a height of 250 km. The intersection of these meridians is the north CG pole, located toward the top of each image.

The images show structures 6300 Å emission in the form of ~800- to 1000-km-diameter patches, and dawn—dusk elongated features drifting in the anti-sunward direction. Patches are observed near the zenith at 07:06, 08:06, 09:33, 10:30, and 11:12 UT. Two dawn-dusk elongated features drifted through the zenith at 07:30 and 08:57 UT. Both types of structures drift in the anti-sunward direction, first appearing on the noon horizon and then disappearing beyond the midnight horizon of the ASIP. During this period, drift velocities ranged from 500 to 1000 m sec^{-1}. These speeds are similar to previously reported anti-sunward plasma drifts mea-

---

9. Weber, E.J., Buchau, J., Eather, R.H., and Lloyd, J.W.F. (1977) Large scale optical mapping of the ionosphere, AFGL-TR-77-0236. AD A051122.

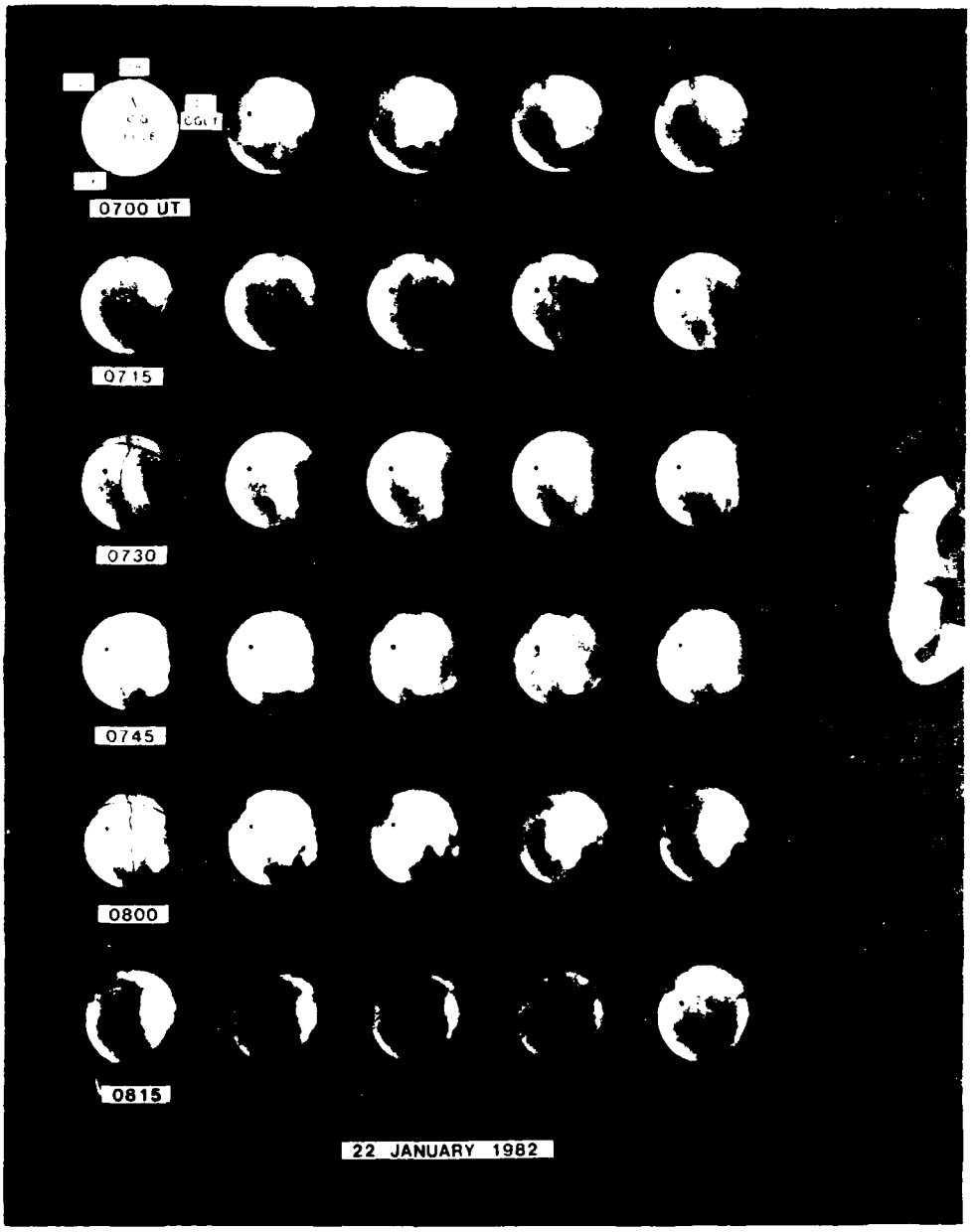

Figure 1a. Sequence of 6300 Å ASIP Images at 3-Min Intervals From 07:03 to 08:27 UT, 22 Jan 1982, From Thule, Greenland (86° CGL). The dawn–dusk (06–18) and noon–midnight (12–00) CG Local Time meridians were projected into the images at a height of 250 km. The intersection of the two meridians is the North CG pole that is at the top of each image. The dot (•) represents the direction to the polar orbiting beacon satellite used for the 250 MHz scintillation measurements

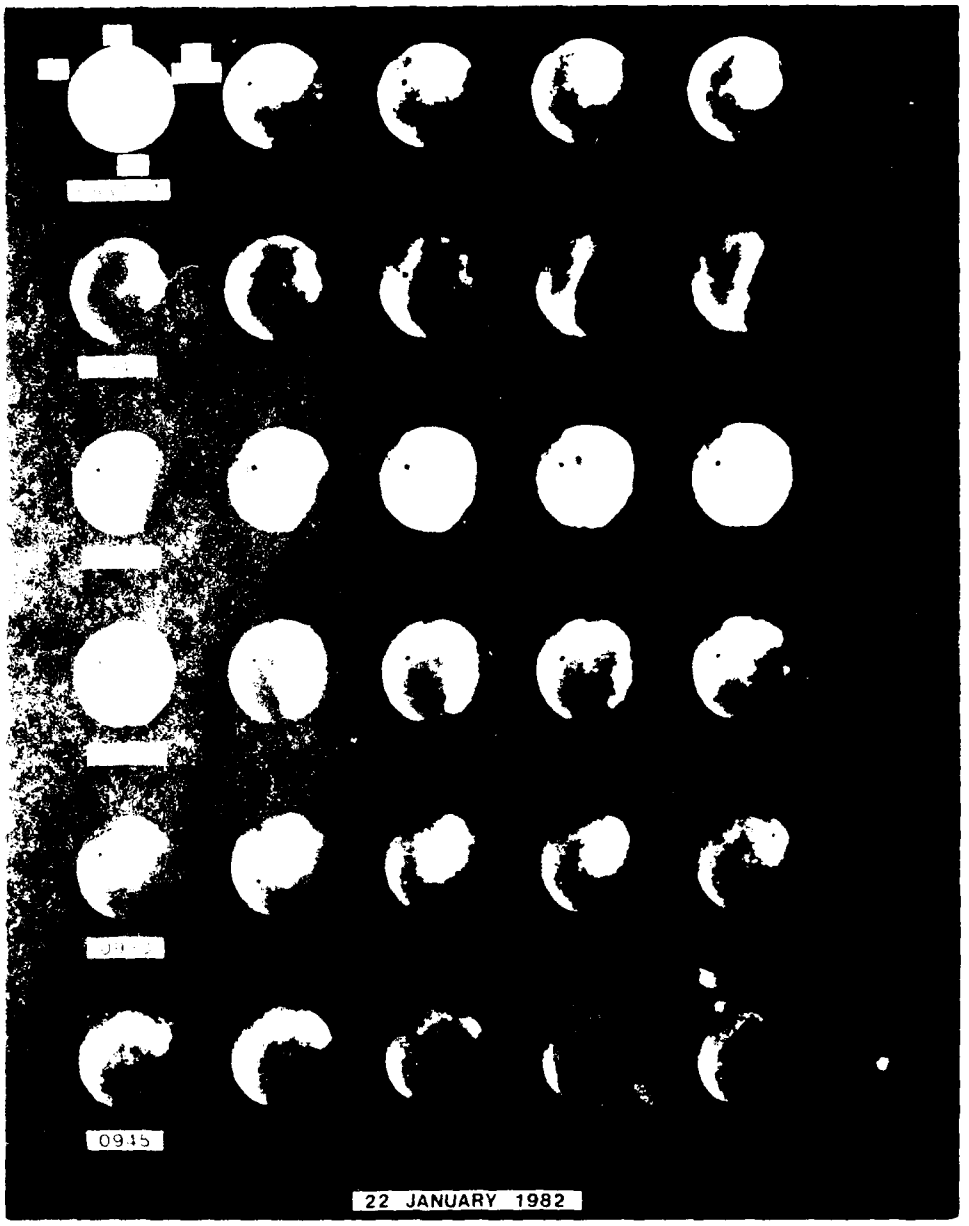

Figure 1b. Sequence of 6300 Å ASIP Images at 3-Min Intervals From 08:33 to 09:57 UT, 22 Jan 1982, From Thule, Greenland (86° CGL). The dawn–dusk (06–18) and noon–midnight (12–00) CG Local Time meridians were projected into the images at a height of 250 km. The intersection of the two meridians is the North CG pole that is at the top of each image. The dot (•) represents the direction to the polar orbiting beacon satellite used for the 250 MHz scintillation measurements

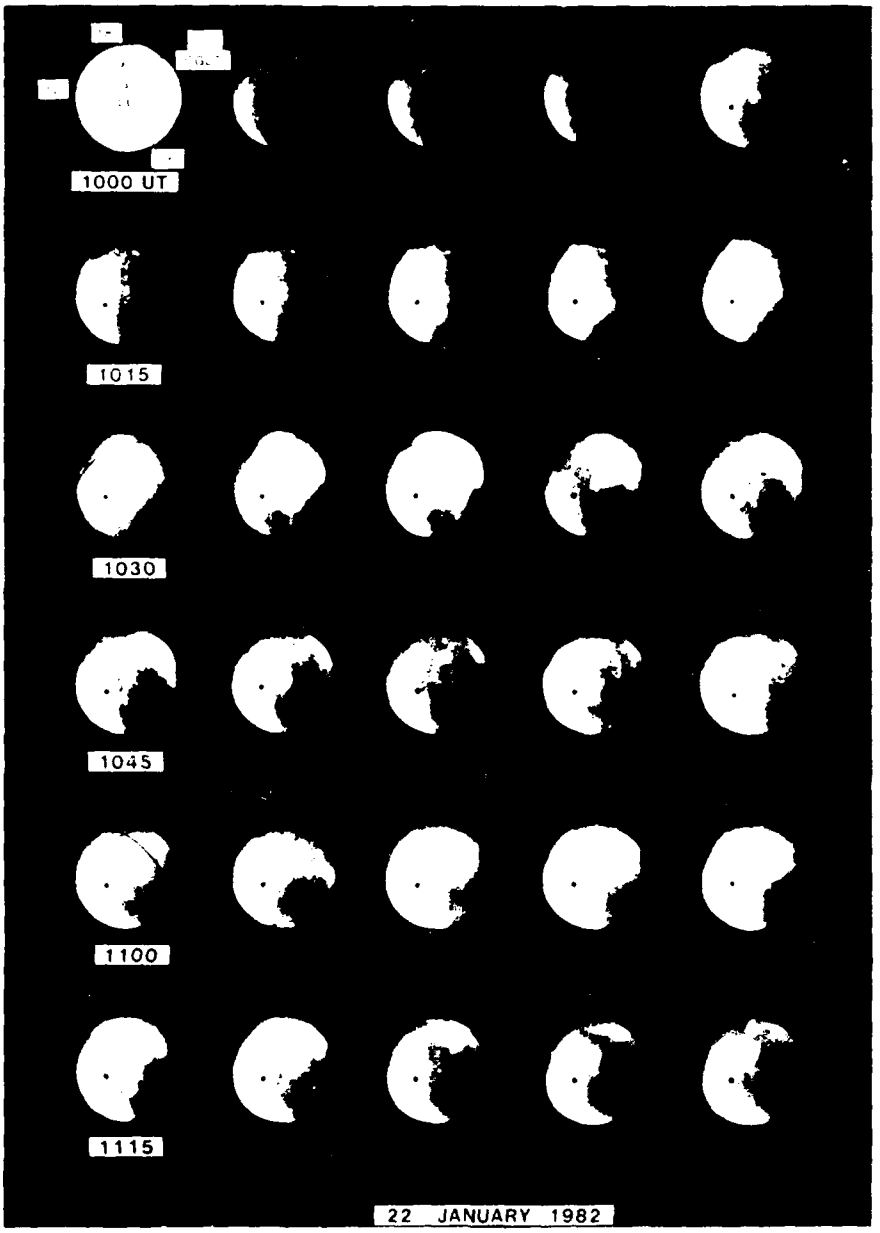

Figure 1c. Sequence of 6300 Å ASIP Images at 3-Min Intervals From 10:03 to 11:27 UT, 22 Jan 1982, From Thule, Greenland (86° CGL). The dawn—dusk (06—18) and noon—midnight (12—00) CG Local Time meridians were projected into the images at a height of 250 km. The intersection of the two meridians is the North CG pole that is at the top of each image. The dot (•) represents the direction to the polar orbiting beacon satellite used for the 250 MHz scintillation measurements

sured by AE—C,[10] and with E x B drift velocities derived from electric field measurements.[11] The images in Figures 1a—1c show a steady glow on the noon horizon near 79° CGL. This is the high latitude edge of the auroral oval in the 06—10 CGLT sector.

The ASIP images provide a measure of the large scale structure and drift of the 6300 Å emission features over a 1200-km region in the polar cap for a comparison with other remote and in situ measurements. To illustrate the quantitative behavior of the optical emission, the 6300 Å zenith intensity measured by a 1 m Ebert-Fastie spectrometer is shown in Figure 2. The 6300 Å emission reached

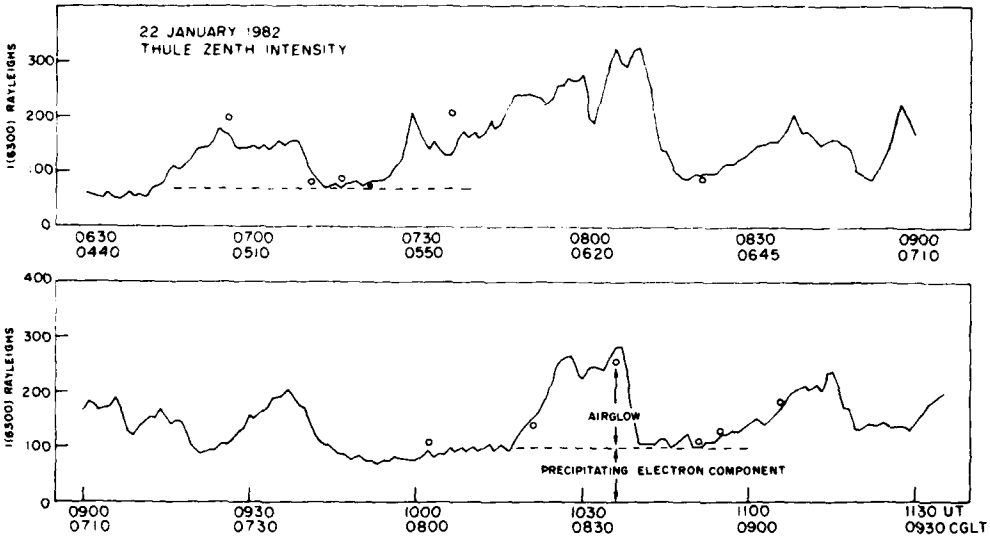

Figure 2. 6300 Å Zenith Intensity From 06:30 to 11:35 UT, 22 Jan 1982, From Thule, Greenland (86° CGL). Also shown are calculated airglow intensities from precipitating electrons (- - -) and from the combined precipitating electron and dissociative recombination components (∘)

maximum values of 200—300R within the patches and decreased to 70—100R in the background ionosphere. The 3914 Å N_2^+ emission was also measured. This did

---

10. Heelis, R.A., and Hanson, W.B. (1980) High latitude ion convection in the nighttime F region, J. Geophys. Res. 85:1995.

11. Heppner, J.P. (1972) Electric field variations during substorms: OGO 6 measurements, Planet. Space Sci. 20:1475.

not vary from outside to inside the patches and showed only a gradual increase with increasing CGLT. The intensity variations will be used in Section 2.3 to separate polar rain excitation (aurora) from the dissociative recombination (airglow) contribution to the total measured 6300 Å intensity.

2.2 Ionosonde Measurements

Ionospheric soundings were performed using a Digisonde 128 PS[12] operated at a rate of one ionogram every 2.5 min. The *Digisonde 128 PS* provides the standard virtual height versus frequency (h'f) information, the amplitudes of the returned signals, and, of special significance for measurements in a highly structured and dynamic environment, the predominant Doppler shift in each frequency-range bin. During these experiments, the Digisonde was operated in a mode to perform Doppler shift measurements over a range of ±22Hz. This Doppler capability allows identification and tracking of drifting F-region irregularity structures in the presence of spread F.

Buchau et al[13] have reported the processing techniques developed for analysis of the Doppler ionograms collected during the January 1982 Polar Cap Campaign. Their analysis showed a positive correlation between bulk drift velocity of polar cap structures and geomagnetic activity (K_p); excellent agreement between instantaneous drift measurements based on the Doppler shift; and the bulk velocities derived from optical imaging data.

Of importance to this study is the capability of separating spread F-ionograms into two sub-ionograms that individually display returns from approaching and receding structures and/or scatterers. A sequence of selected ionograms recorded during the transit of the patch observed from 10:06 to 10:41 UT on 22 January 1982 (see Figures 1a–1c) is shown in Figure 3: B shows the sub-ionograms with negative-Doppler shift (from receding structures), and C, those with positive-Doppler shift (from approaching structures). The ionograms in Figures 3 and 4 show a quasi-analog presentation of the Doppler shift associated with each echo, instead of the more commonly used echo amplitude. Low-Doppler shifts appear as light gray, and high-Doppler shifts appear darker.[14]

The sequence of ionograms shown is typical for the approach of an ionization patch and its transit through the zenith. In Figure 3, A shows the corresponding

---

12. Bibl, K., and Reinisch, B.W. (1978) The universal digital ionosonde, Radio Sci. 13:519.
13. Buchau, J., Reinisch, B.W., Weber, E.J., and Moore, J.G. (1983) Structure and dynamics of the winter polar cap F region, Radio Sci. (in press).
14. Patenaude, J., Bibl, K., and Reinisch, B.W. (1973) Direct digital graphics, American Lab. 15:95.

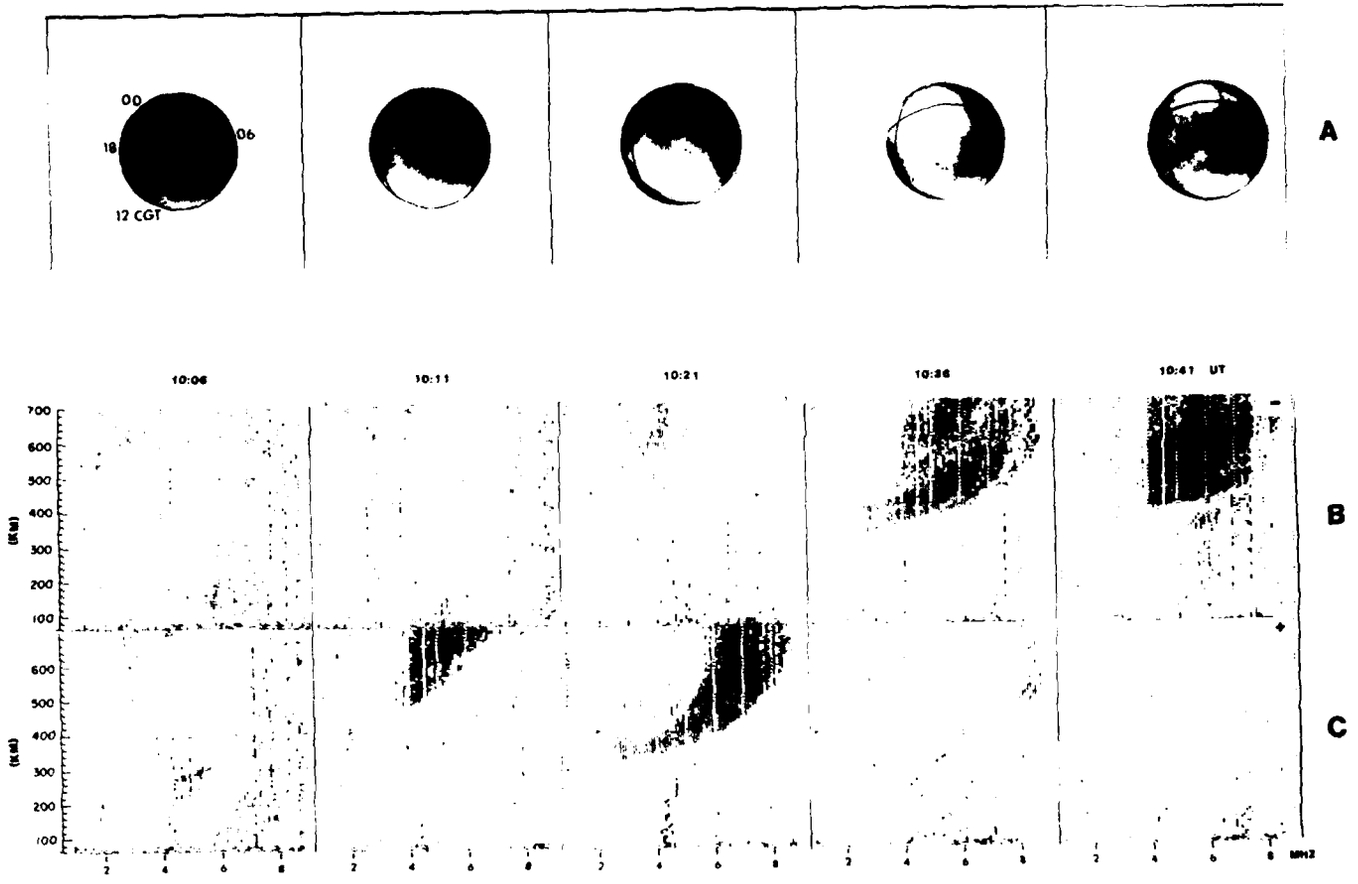

Figure 3. Sequence of 6300 A ASIP Images From 10:06 to 10:41 UT, 22 Jan 1982, From Thule, Greenland (86 CGL), Showing Anti-Sunward Drift of an Airglow Patch (A), Corresponding Negative-Doppler (B), and Positive-Doppler Digital Ionograms (C) to Illustrate F-Layer Ionization Characteristics Associated With the Patch

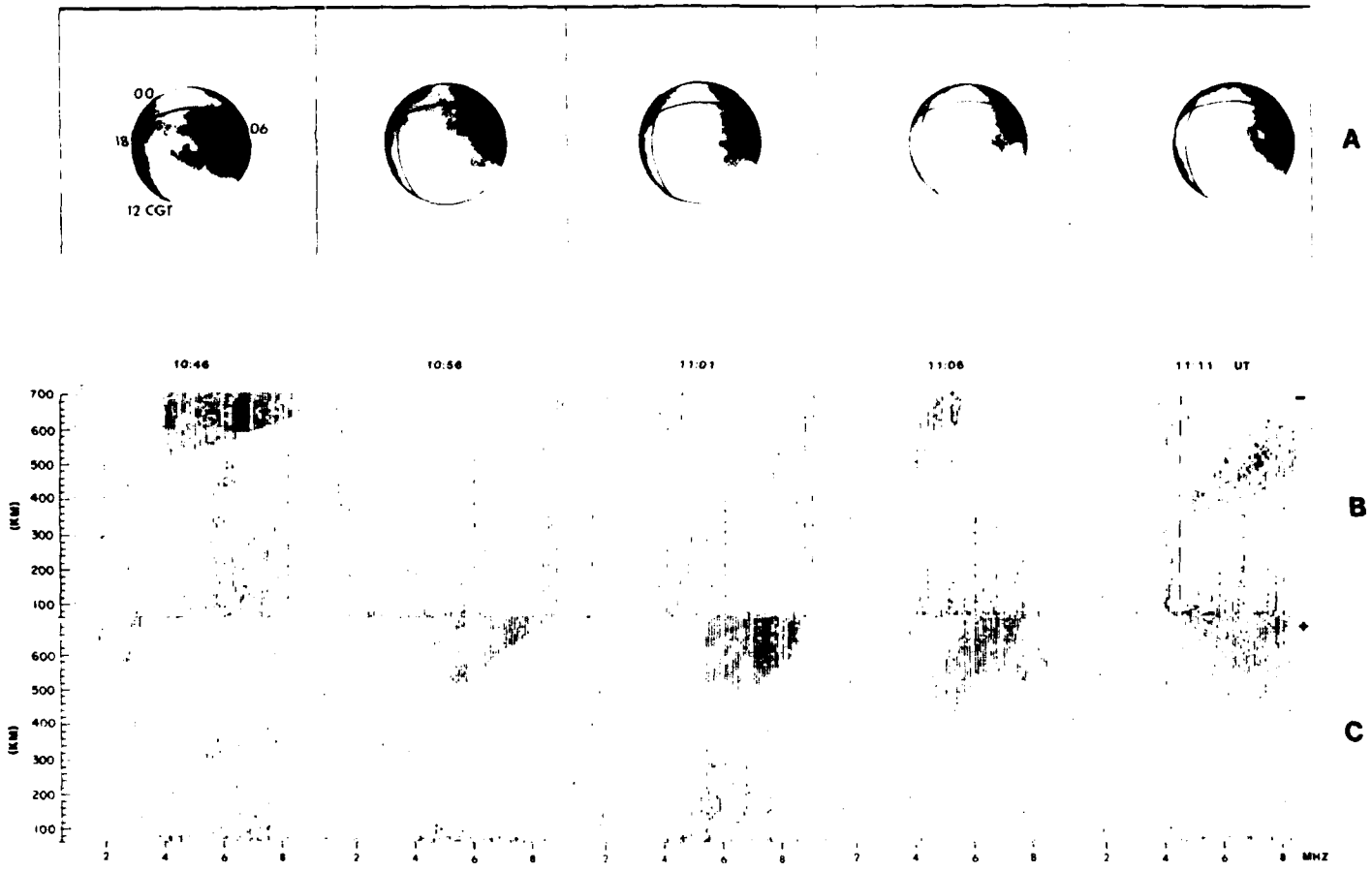

Figure 4. Sequence of 6300 A ASIP Images From 10:46 to 11:11 UT, 22 Jan 1982, From Thule, Greenland (86 CGL), Showing Anti-Sunward Drift of an Airglow Patch (A), Corresponding Negative-Doppler (B), and Positive-Doppler Digital Ionograms (C) to Illustrate F-Layer Ionization Characteristics Associated With the Patch

6300 Å ASIP images, the noon—midnight meridian is aligned along the left horizon. The 10:06 UT image shows, as discussed in Section 2.1, the high latitude edge of the auroral oval in the 06—10 CGLT sector on the sunward horizon. A patch, hereafter called patch A, moved out of that region in the anti-sunward direction. The leading edge arrived in the zenith at ~10:21 UT. By 10:36 UT, the trailing edge of the patch was just crossing the zenith. In the last image, taken at 10:41 UT, the patch had moved approximately halfway out of the field-of-view towards midnight.

The positive-Doppler ionogram at 10:06 UT shows a typical low-density nighttime F-region with an foF2 $\approx$ 2.8 MHz (corresponding to $N_e max = 9.7 \times 10^4$ el cm^{-3}). The small area of high-Doppler shift between 4.2 and 5.8 MHz, starting at a range of ~210 km, shows rangefolded returns from a reflecting/scattering structure at a virtual range of approximately 960 km. Since the sounder operated at a pulse repetition frequency of 200 Hz, returns from ranges larger than 750 km are rangefolded into the primary 750 km range. Phase coding of the transmitted hf signals and proper decoding in the receiver reject all but very strong overrange echoes. This overrange return is the first indication of the approaching ionization patch. The ionograms taken at 10:11 and 10:21 UT clearly show the ionospheric signatures of the rapidly approaching patch. At 10:11 UT, high-Doppler returns are observed in the positive-Doppler ionogram at ranges $\geq$ 460 km. By 10:21 UT, the leading edge of patch A has reached the zenith. This is determined from the low-frequency trace (foF2 ~ 4 MHz, $N_e max = 2.0 \times 10^5$ el cm^{-3}) observed at essentially zero Doppler in both the positive and negative sub-ionograms. The heavy spread-F trace with high positive-Doppler, simultaneously observed at 10:21 UT, suggests that the major part of patch A is still approaching. This is clearly supported by the 10:21 UT ASIP image, which shows a 6300 Å substructure in the zenith at the edge of a large approaching airglow region.

By 10:36 UT, this airglow region (patch A) has almost completely passed through the zenith, and the corresponding ionogram shows most of the ionospheric returns with strong negative-Doppler. However, the signature of the ionization in the trailing region of the patch produces a clear virtual height trace in the ionogram with low positive-Doppler and an foF2 = 8.0 MHz ($N_e max = 8 \times 10^5$ el cm^{-3}). Since the echo amplitudes from overhead and slightly off-vertical regions differ very little, the overhead traces could only be identified using their Doppler signatures. Finally, the ionogram at 10:41 UT now shows all returns appearing in the negative-Doppler ionogram at ranges $\geq$ 390 km. This suggests that the ionization patch has moved away from the zenith, as observed in the corresponding ASIP image. The weak trace (low Doppler) in the negative-Doppler ionogram shows the low-density overhead ionosphere with foF2 < 3 MHz.

The approach of the next patch, hereafter called patch B, is shown in Figure 4.

The ASIP images (A) show patch A low on the midnight horizon at 10:46 UT, and patch B, a new patch, moving out of the noon sector. By 11:01 UT, patch B was centered over the station. The ionogram at 10:46 UT shows the rapidly disappearing patch A visible in C. The overhead ionosphere is again very weak (foF2 $\approx$ 3.0 MHz). At 10:56 UT, patch A had moved out of the range of the ionosonde (and cut of the field-of-view of the ASIP), while strongly enhanced and spread returns from patch B approached. By 11:01 UT, the leading edge of patch B with an foF2 $\approx$ 4 MHz is overhead, and the ionogram at 11:06 UT shows evidence of strong electron density enhancement (foF2 $\approx$ 8 MHz) in the negative-Doppler panel. By 11:11 UT, no distinct traces are obtainable, even though cusp-type structures in both the negative- and positive-Doppler ionograms indicate the presence of strongly enhanced and structured ionization in patch B, now in the zenith.

It should be pointed out here that the ability to separate signatures of ionospheric profiles or structures is most effective close to the leading or trailing edge of patches. In this case, most of the echo returns from the larger patch structure are separated from the signature of the overhead ionization by different Doppler shifts.

To establish the two-dimensional structure of a patch, a sequence of clearly identifiable ionogram traces was taken from all ionograms recorded during the transit of patch A up to the arrival of the leading edge of patch B. True-height analysis was performed using these traces. Since no E-region returns were observed during this period, the starting height of the ionization was set at 180 km. An upper limit for the ionization density at E-region heights can be set at $\leq 10^4$ el cm^{-3}, based on a combined assessment of the ionograms, the measured particle precipitation, and the 3914 A N_2^+ zenith measurements. Setting this low E-region density to zero for the true-height analysis only slightly affects the resulting F-region profiles, and has no substantial impact on our conclusions.

Constant electron density contours along the noon–midnight axis of patch A are shown in Figure 5. The sequence of ASIP images indicated a horizontal velocity of $\sim$ 700 m sec^{-1} determined from the Doppler measurements. Since the ionosonde measures Doppler shift—that is, the radial velocity component—more exact velocity measurements require knowledge of the height of the scattering or reflecting region and the exact raypath. Using a velocity of 700 m sec^{-1}, the spacing of the ionograms in the horizontal direction could be determined. They are indicated by the respective UT markers above the abscissa. It should be noted that the abscissa has twice the resolution of the ordinate. A topside profile using a modified Chapman layer[15] has been matched to each bottomside profile to provide the necessary input to the computation of the 6300 Å emission in Section 2.3.

15. Tinsley, B.A., Christensen, A.B., Bittencourt, J.A., Angreji, P.D., and Takahashi, H. (1973) Excitation of oxygen permitted line emissions in the tropical nightglow, J. Geophys. Res. 78:1174.

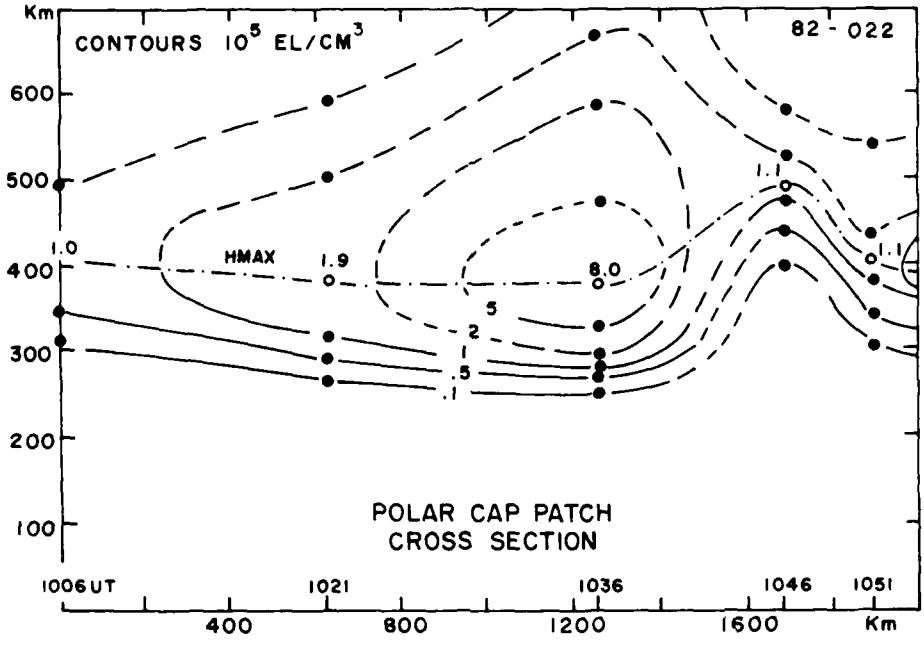

Figure 5. Electron Density Contours Along the Noon—Midnight Axis of the Ionization Patch Observed From 10:06 to 10:51 UT, 22 Jan 1982, From Thule, Greenland (86° CGL). The horizontal scale was determined using the measured drift velocity of 700 m sec^{-1}. Computed values obtained from the true height analysis are indicated on the equi-density contours (•). The height of $N_e$max, the maximum density of the F-layer patch at this location, are also represented (∘). The section of the bottomside contours between 10:36 and 10:46 UT (- - -) indicates uncertainty of the exact profiles in this region. The leading edge of patch B is also shown.

The resulting cross-section shows a localized eightfold enhancement of electron density above the background ionization of $\leq 10^5$ el cm^{-3}. The horizontal dimension is ~ 1200 km. The leading edge of the patch has a horizontal gradient scale length $L \geq 230$ km where $L = \left(\frac{1}{N}\frac{\partial N^{-1}}{\partial X}\right)^{-1}$ while the trailing edge is steeper, $L \approx 100$ km. Uncertainty of the exact profiles in this region is indicated in the bottomside contours between 10:36 and 10:46 UT. There is some indication that the ionization drops well below the 1.1×10^5 el cm^{-3} measured at 10:46 UT; therefore, the N_e gradient on the trailing edge might be considerably larger. Figure 5 also shows the leading edge of patch B.

The transit of a patch at a velocity of 700 m sec^{-1} leads to rapid changes in the observed minimum virtual range or height from overhead and oblique returns in the ionogram. The Integrated Height Characteristic shown in Figure 6, produced by collapsing each amplitude ionogram onto its height axis, permits a quick survey of the height variation over extended periods. Figure 6 contains approximately

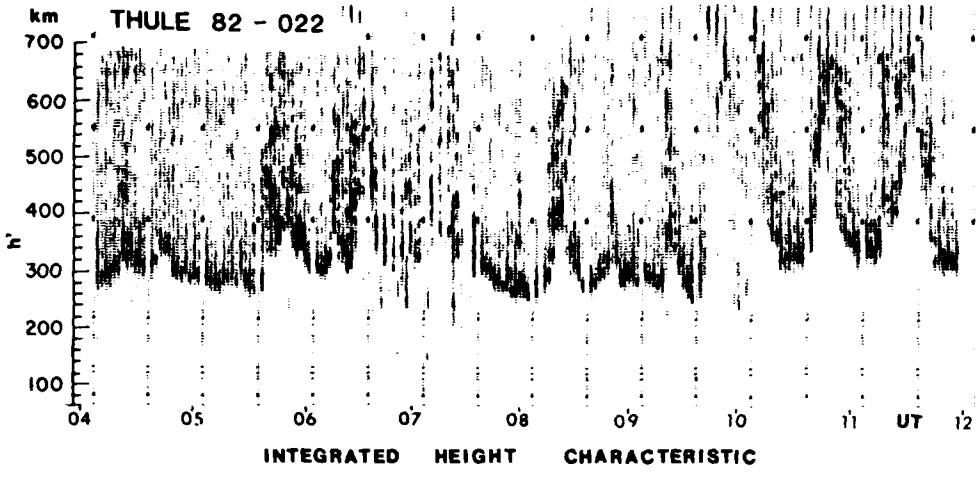

Figure 6. Integrated Height Characteristic Using Both Positive- and Negative-Doppler Ionograms for 22 Jan 1982. The lower boundary of the heavy, dark trace represents h'(t), which changes by as much as 400 km in 15 min

200 ionograms for 8 h of observations and shows changes in height by as much as 400 km in 15 min. These fast transitions are the signatures of the strongly enhanced ionization patches moving rapidly in a background of very low density. The optical patches reported in the zenith at 08:06, 09:33, and 10:30 (patch A), and 11:12 UT (patch B) are easily identified in the Integrated Height Characteristic. Patches A, B, and a last one which reached the zenith at ~ 11:50 UT are especially identifiable individually over distances larger than 1000 km because of their large separation. The slope of the range change during approach and retreat characterizes the bulk motion of the patch ionization and corresponds to velocities $\geq$ 600 m sec^{-1}. These are in good agreement with the optical and Doppler measurements, considering that no refraction effects have been taken into account.

2.3 Precipitating Particle Characteristics

Precipitating particle measurements from the Low [illegible] Plasma Instrument (LAPI) on DE—2 were available for 22 January 1982 [illegible] passes [illegible] at 06:55, [illegible], and 10:07 UT for comparison with [illegible] events. The 06:55 UT pass was within 109 [illegible] of Thule [illegible] comparison between particle fluxes and optical emissions. Figure 7 [illegible] differential energy flux, in spectrogram form, for [illegible] pitch angle. From these data, the polar cap [illegible] spectrogram between 06:52:25 UT (78.4 [illegible]), 0.00 [illegible] UT [illegible] 07:01:00 UT (74. [illegible]), [illegible]

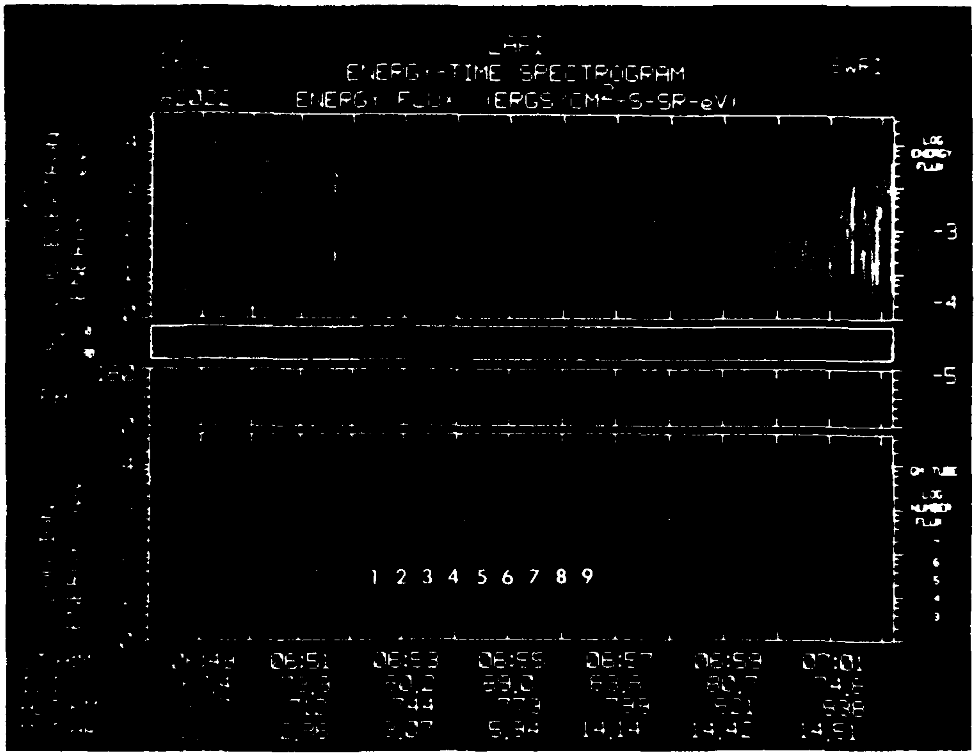

Figure 7. Energy-Time Spectrogram on the 06:55 UT Pass of DE—2 Satellite Over the Northern Polar Cap on 22 Jan 1982, Showing Electrons and Ions at 46 Pitch Angle and Geiger Counter Measurements of the LAPI. The polar cap lies between 06:52:25 UT (78.4° [illegible]) and 07:01:00 UT (74.3° [illegible]). The distance of closest approach of the sub-satellite point to Thule was 109 km and occurred at 06:54:37 UT.

MLT). In this region, only soft electrons are observed. Their spectral peak energy is ~ 100 eV.

The 6300 Å ASIP image at 06:54 UT is shown in Figure 8. To compare the

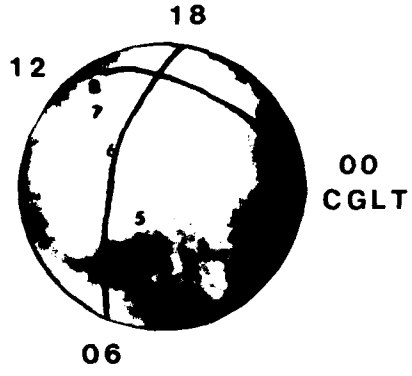

Figure 8. 6300 Å ASIP Image at 06:54 UT, 22 Jan 1982, From Thule, Greenland (86~CGL). The numbers 1—9 in the ASIP image are the positions of the magnetic field line traced from satellite altitudes down to the 250-km interaction height

particle and optical data, the satellite position at each half-minute, beginning with 06:52:30 UT, was traced downward using the 1980 IGRF model from the satellite altitude (735—790 km) to an approximate loss height of 250 km. These positions were then plotted into the ASIP image. The numbers 1—9 in the ASIP image correspond to the same numbers in the spectrogram (see Figure 7). Although the polar cap precipitation is not completely uniform, the small variations do not correspond to the ~ 1000-km scale size of the patches seen in the 6300 A image.

This comparison suggests that the localized 6300 A patches seen in the ASIP images and in the intensity variations in Figure 2 are not produced by direct particle precipitation, but are primarily airglow structures produced by patches of enhanced F-region ionization. The motion of the features suggests that this ionization is not locally produced but is observed after production as it convects across the polar cap in the anti-sunward direction. During the period of observation, this ionized patch undergoes chemical recombination which results in the 6300 A airglow.

To test this hypothesis, the total 6300 Å emission (direct excitation from precipitating electrons plus airglow from dissociative recombination) has been estimated for patches near the aircraft zenith during the DE—2 passes at 06:55 and 10:07 UT. The quantitative behavior of these patches is clearly seen in the 6300 Å intensity measurements in Figure 2. The first patch under consideration drifted through the spectrometer field-of-view from 06:40 to 07:12 UT; the second patch, from 10:18 to 10:40 UT.

2.3.1 FIRST PATCH

The electron spectra at 06:55:27 UT were used to calculate the contribution from the polar rain and from photoelectrons produced below the satellite (Figure 9).

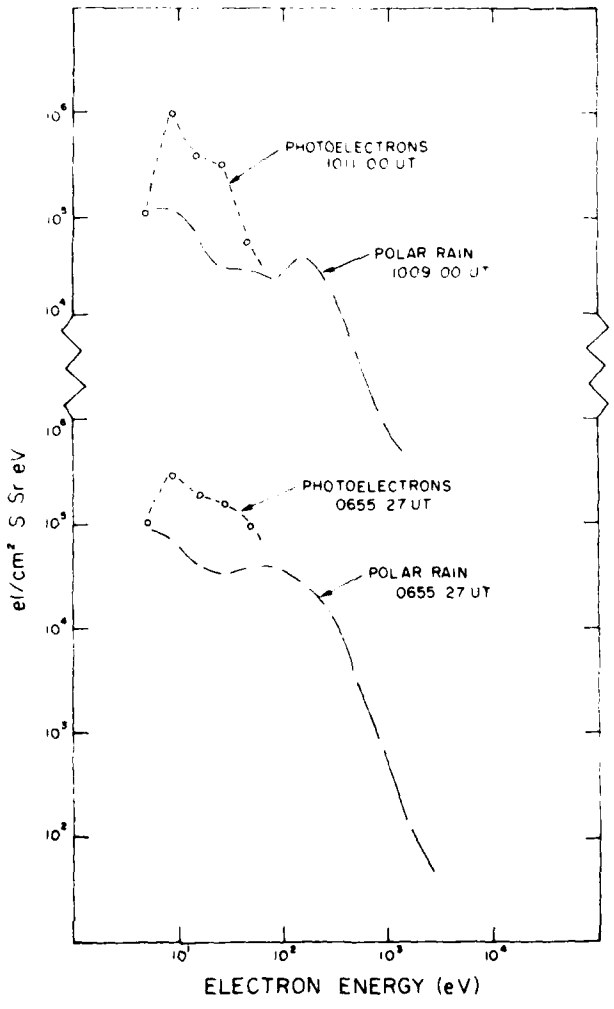

Figure 9. Electron Sources of 6300 Å Emission and F-Layer Ionization Showing Polar Rain and Photoelectron Spectra at the Nearest Approaches of the Subsatellite Point to Thule, Greenland, During the 06:55 and 10:07 UT Passes

For the polar rain contributions, spectra were averaged over the 62° loss cone using detectors at 9°, 46°, and 61°. The photoelectrons, such as those described by Winningham and Gurgiolo,[16] are produced by scattered UV radiation below the satellite and are distributed isotropically. They are detected at satellite altitude in the upcoming (136° pitch angle) detectors at energies between 5 and ~ 60 eV. Since they are isotropic, similar fluxes are expected to precipitate into the F layer and contribute to 6300 Å emission. The polar rain and photoelectron fluxes of Figure 9 have been added to obtain an effective spectrum representing the total particle flux incident on the F layer. The auroral ionization/emission model* based on the electron transport code of Strickland et al[17] was used to calculate the expected 6300 Å emission and the electron density profile from the incident spectrum. The calculated value of 70R is shown as a base level in Figure 2, since the polar rain fluxes did not show significant spatial variation in the vicinity of Thule.

The airglow contribution was calculated using true height bottomside profiles from the digital ionograms.[18] These were matched at the F-layer peak to a modified Chapman function[15] to extend the profile above the peak to 650 km. The calculation of the 6300 Å airglow from charge exchange of O^+ with O_2 followed by dissociative recombination of O_2^+ is identical with the method outlined in Weber et al.[19] Airglow intensities were calculated whenever a reliable true height profile could be derived from the ionogram. Spread F at other times precludes the derivation of true height profiles. The calculated airglow intensities plus precipitating electron contributions are shown in Figure 2. These agree to within 30R of the measured values both within and outside the patch. This comparison indicates that the background level of 6300 Å emission is due to precipitating electrons, and the increases above background are due to airglow production within the high density patches.

Although the electron spectrum can account for the 6300 Å emission outside the patch, the ionization production (and resulting electron density profile) from

---

*Strickland, D. J. Private communication.

16. Winningham, J. D., and Gurgiolo, C. (1982) DE-2 photoelectron measurements consistent with a large scale parallel electric field over the polar cap, Geophys. Res. Lett. 9:977.

17. Strickland, D. J., Book, D. L., Coffey, T. P., and Fedder, J. A. (1976) Transport equation techniques for the deposition of auroral electrons, J. Geophys. Res. 81:2755.

18. Reinisch, B. W., and Huang Xueqin (1983) Automatic calculation of electron density profiles from digital ionograms, 3. Processing of bottomside ionograms, Radio Sci. 18:3.

19. Weber, E. J., Brinton, H. C., Buchau, J., and Moore, J. G. (1982) Coordinated airborne and satellite measurements of equatorial plasma depletions, J. Geophys. Res. 87:10503.

this spectrum is not sufficient to account for the measured electron density in the background ionosphere. Figure 10 shows electron density profiles inside and outside the F-layer patch determined from the ionograms. Also shown is the electron

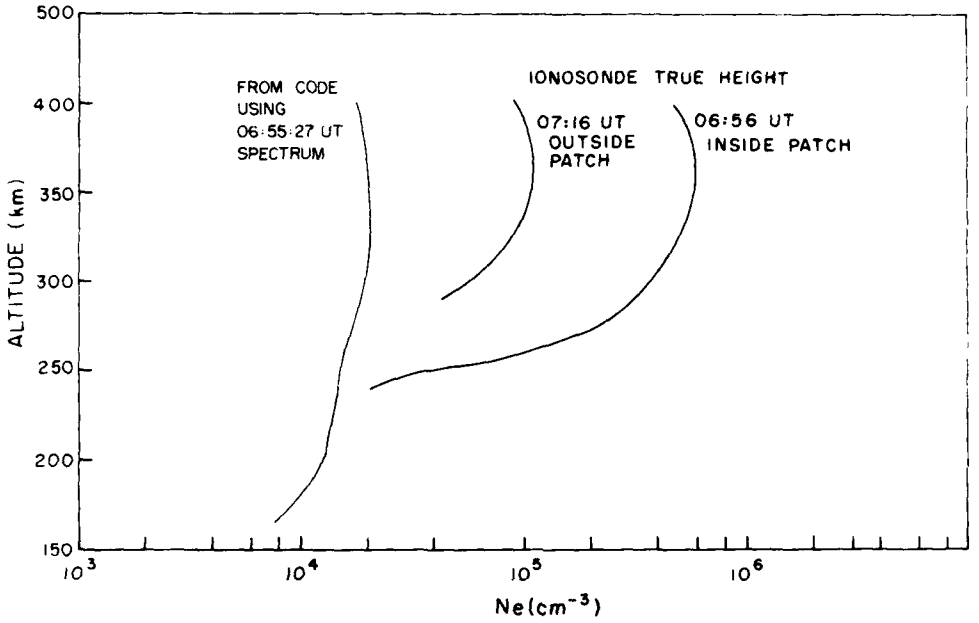

Figure 10. Electron Density Profiles Inside and Outside the F-Layer Patch Determined From True Height Analysis of Ionograms. Also shown is the profile expected from soft electron precipitation into the polar cap

density profile from the numerical code using the composite spectrum in Figure 9. The measured background density is almost one order of magnitude larger, and the layer peak is found at higher altitudes than the profile resulting from the numerical calculation, showing that local fluxes are not sufficient to produce the measured polar F-layer density. This suggests that the entire observed ionosphere (patches plus background) is transported into the polar cap from a source region within or equatorward of the dayside auroral zone.

2.3.2 SECOND PATCH

The energy-time spectrogram for electrons at pitch angles of 46° and 136° on the 10:07 UT pass is shown in Figure 11. As was the case during the 06:55 UT pass, the polar cap electron precipitation is unstructured and low in energy. Since the satellite passed 880 km to the west of Thule on this pass, direct comparison within a common ionospheric volume was not possible. In an attempt to represent

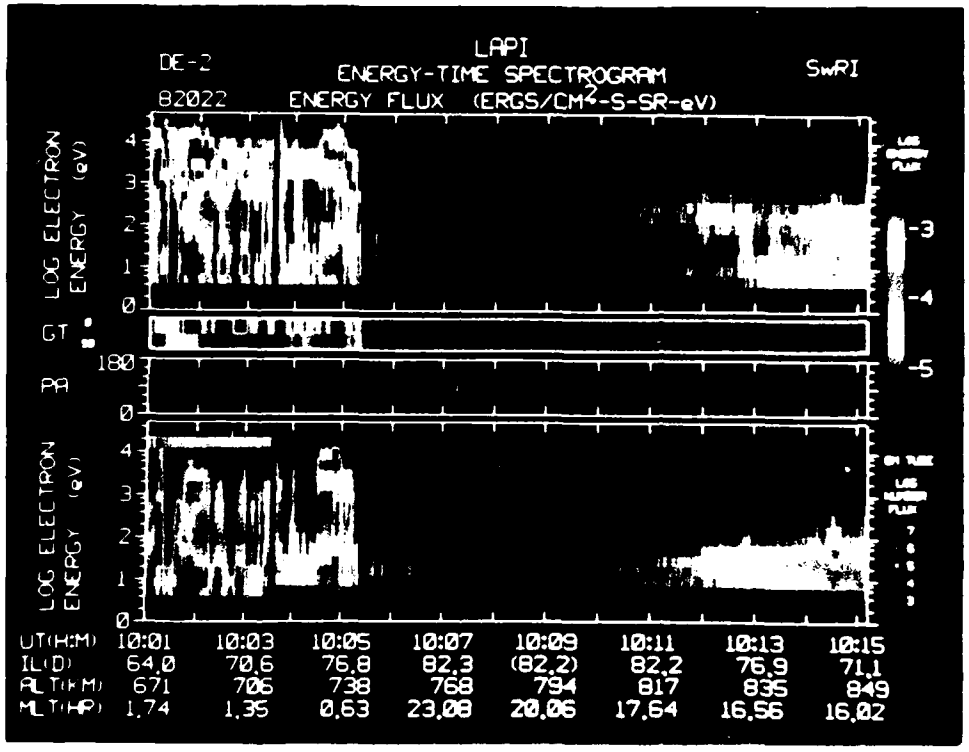

Figure 11. Energy-[illegible] Polar Cap on 22 [illegible] ward electron fluxes at 16 [illegible] respectively

accurately the fluxes at Thule, the polar rain spectrum was selected at a time when the satellite was nearest Thule's geomagnetic latitude (10:09:00 UT in Figure 11); however, the photoelectron spectrum was selected at a time when the shadow height at the satellite location was 800 km, the same as that above Thule (10:11:00 UT in Figure 11). These spectra are shown in Figure 9, and, as in the 06:55 UT pass, they have been added to obtain an effective spectrum incident on the F-layer. When used in the ionization/emission code, the result is a calculated value of 6300 Å emission of 92R. This is in good agreement with the observed value of 100R outside the patch and suggests little spatial variation in the polar rain between Thule and the DE—2 Field line.

Calculation of the airglow component of this patch used the true height profiles shown in Figure 5. Since the calculated and measured background intensity differ slightly, we used the locally measured value of 100R as a baseline and added to it the calculated airglow intensity, shown in Figure 2 for the patch near the zenith from 10:17 to 10:40 UT. Using the 100R background, the calculated airglow values show excellent agreement with the measured intensities.

These comparisons of LAPI data with measured airglow and electron densities confirm that the ionization patches are not locally produced, but are transported into the polar cap from a source region upstream in the E x B convective flow pattern. In addition, the polar rain fluxes are not sufficient to account for production of the background ionization between the patches. This plasma, therefore, must also be transported into the polar cap. Possible source regions are discussed in Section 3.

2.4 Intermediate Scale Structure

The large scale patches seen optically and with the sounder are subject to instability processes that will produce intermediate scale (few kilometers and smaller) irregularities. To characterize these secondarily produced irregularities, complex signal radio-wave scintillation measurements were made throughout the 21—27 January period. The signal sources for these observations were polar orbiting beacons in highly eccentric orbits that transmit at 250 MHz. These appear at high elevation angles for extended periods over Thule, and provide near-continuous raypath penetrations through the central polar cap F-region. The information provided by the complex signal data includes the irregularity strength at spatial scales from a few kilometers to about 100 m[20] and, through the use of spaced re-

---

20. Rino, C.L. (1982) On the application of phase screen models to interpretation of ionospheric scintillation data, Radio Sci. 17:855.

ceivers, the irregularity anisotropy and drift.[21] Thus, we can establish the spatial association between the irregularities and the macroscale patches and determine their relative motion.

The measured signal intensity scintillation index, S_4, is plotted in Figure 12 for the period of interest. It is a good first-order indicator of irregularity occur-

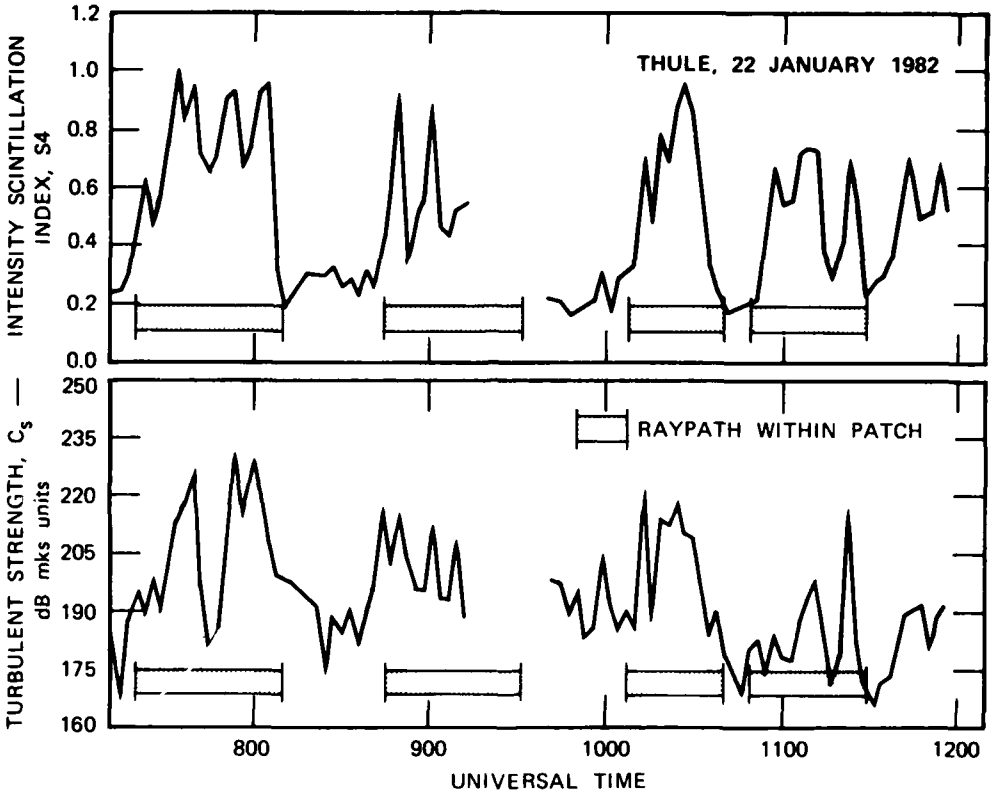

Figure 12. Intensity Scintillation Index (S_4) and Turbulence Strength (C_S) for 22 Jan 1982. Times when the signal raypath was within an F-region patch are indicated

rence, and comparison with the raypath penetration points shown in Figures 1a–1c shows that there is a clear association between the patches and kilometer-scale structure. When the raypath passes through the high density patches, the S_4 index

21. Rino, C.L., and Livingston, R.C. (1982) On the analysis and interpretation of spaced received measurements of transionospheric radio waves, Radio Sci. 17:845.

approaches saturation ($S_4 \sim 1$), while the intervening low-density regions produce only weak signal variations. To illustrate this correlation more clearly, times when four major optical patches intersected the satellite raypath between 07:00 and 12:00 UT are indicated on Figure 12.

The complex signal data also makes it possible to obtain a measure of the absolute density turbulence in the patches. This is because the signal phase provides a near-direct mapping of the irregularity continuum for the scintillation conditions of interest in this case.[20] The turbulence estimates are made using phase scintillation spectral parameters as outlined in Livingston et al,[22] and the irregularity anisotropy and drift that are measured directly using spaced receivers.[21] The resulting estimate of three-dimensional turbulent strength, C_s, is shown in Figure 12. The S_4 index and C_s generally track, as they must, but C_s provides a measure of the true dynamic range of the density turbulence.

For example, if we assume a constant irregularity layer thickness, the structuring or turbulence on the sunward edges of the patches is some 30 dB stronger than that in the low-density background regions. It is interesting to note that the peak C_s levels in Figure 12 correspond to median levels observed at the magnetic equator during moderate sunspot conditions.[22]

The data in Figure 12 also provide information about the instability mechanism that is producing the km-scale structure. The first, third, and fourth patches—that is, those isolated and clearly defined—show a systematic difference in the severity of scintillation on their leading and trailing edges. The scintillation produced by irregularities within the trailing (sunward) edge always exceeds that produced by irregularities with the leading (anti-sunward) edge. This asymmetry compares well with the electron-density contours determined from the ionograms (Figure 5), and with the zenith 6300 Å intensities, which show a slow rise followed by a steep drop (Figure 2). Combined, these observations suggest that it is the gradient drift instability[23] that produces the secondary structuring within the patches.

The irregularity drift during this same period as measured by the spaced-receiver method is shown in Figure 13. The motion is anti-sunward, with a small component towards the dawn sector. During the passage of the 10:20 UT patch through the line of sight, the velocity is about 600 m sec^{-1}, in good agreement with the drift velocity of the overall patch estimated from optical and sounder measurements. There is a general increase in the velocity between dawn and noon at these

---

22. Livingston, R.C., Rino, C.L., McClure, J.P., and Hanson, W.D. (1981) Spectral characteristics of medium-scale equatorial F region irregularities, J. Geophys. Res. 86:2421.

23. Linson, L.M., and Workman, J.B. (1970) Formation of striations in ionospheric plasma clouds, J. Geophys. Res. 75:3211.

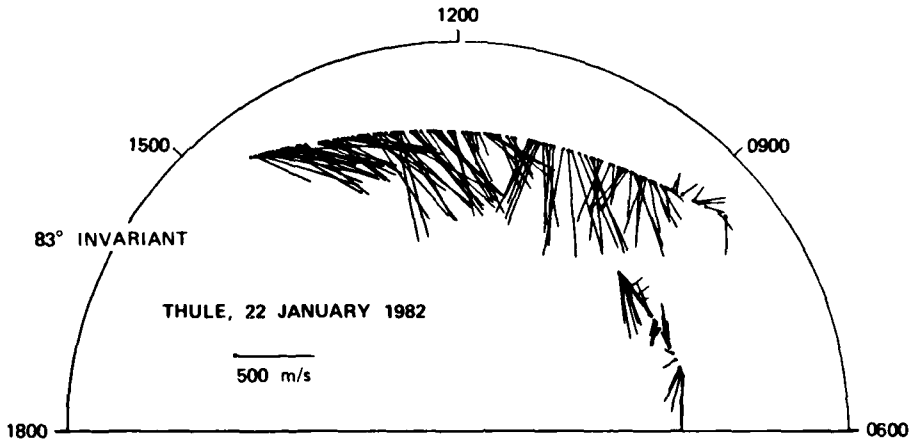

Figure 13. CGL/Local Time Plot Showing Irregularity Drift Pattern Determined From Spaced-Receiver Scintillation Measurements

latitudes, in agreement with the models of two-celled convective plasma flow in the polar cap.[24] Drift of the neutral atmosphere, which results primarily from ion drag at this season and latitude, will follow the same flow pattern but will lag the plasma by an hour or more. In the morning sector, the result is that the anti-sunward plasma flow will be more rapid than the neutral flow. As discussed by Linson and Workman[23] for Barium cloud striations, irregularity generation is expected in regions where the ion-drift velocity vector and electron-density gradient are parallel. In the reference frame of the neutrals, therefore, it is the sunward edge of the patches that are gradient-drift unstable; here, the drift and gradient vectors are parallel, resulting in steepening and eventual structuring. Using the measured parameters of V_{patch} = 700 m sec^{-1}, L = 100 km and an expected neutral wind speed between V_n = 100—200 m sec^{-1} in the anti-sunward direction[25] gives a growth time $\tau(^{L}/V_{patch} - V_{neutral})$ of ~170—208 sec near the F-layer peak on the trailing edge of this patch. Although the trailing edge of the patch contains the

24. Heelis, R.A., Lowell, J.A., and Spiro, R.W. (1982) A model of the high-latitude ionospheric convection pattern, J. Geophys. Res. 87:6339.

25. Roble, R.G., Dickinson, R.E., and Ridley, E.C. (1982) Global circulation and temperature structure of thermosphere with high latitude plasma convection, J. Geophys. Res. 87:1559.

most intense irregularities, the entire patch structure is populated with km-scale irregularities of sufficient intensity to produce saturated uhf-amplitude scintillation. This is to be expected since the gradient-drift mechanisms will eventually structure a large fraction of the original patch.

3. CONCLUSIONS

Coordinated ionospheric measurements have shown the existence of large patches of enhanced ionization drifting across the polar cap in the anti-sunward direction during moderately disturbed ($K_p \geq 4$) geomagnetic conditions. The patches (~ 800—1000 km diameter) were initially observed as they separated from the morning sector of the auroral oval. Drift speeds ranged from 500—1000 m sec^{-1} corresponding to a dawn—dusk electric field strength of 25—50 mV m^{-1}. Simultaneous DE—2 LAPI measurements show no direct precipitating particle source for these regions of increased ionization. In addition, the polar rain fluxes are not sufficient to produce the background densities observed between the patches.

This comparison suggests that all of the polar cap ionization (patch plus background) was produced further upstream in the high-latitude convection-flow pattern. Possible source regions include ionization produced in the sunlit ionosphere and transported into the polar cap by E x B drift. Another possibility is a source region associated with convection through the dayside aurora/cusp precipitation region. In either case, the source region and transport mechanism must account for the non-uniform distribution of plasma and the high peak-density (10^6 cm^{-3}). Steady convection through the cusp region, for example, would not produce the discrete patches seen in the polar cap. Estimates made by Knudsen[26] indicate that direct convection through the cusp would add ~ 2 x 10^5 el cm^{-3} to the density near the peak of the F layer. This may be a source for the background polar F-layer, which has a density comparable to that expected from the cusp. Direct convection through the cusp, however, does not result in the large densities observed in the patches. A possible mechanism would be sunward convection along the cusp for tens of minutes before the anti-sunward flow across the polar cap. This "spatial resonance" would allow sufficient time for the electron density to build up to ~ 10^6 el cm^{-3}.

Alternatively, spatial/temporal variations in the high-latitude electric field may periodically attach solar produced sub-oval (corotating) plasma (N_{max} ~ 10^6 el cm^{-3}) to the E x B convective flow system. Subsequent drift

---

26. Knudsen, W.C. (1974) Magnetospheric convection and the high latitude F_2 ionosphere, J. Geophys. Res. 79:1046.

would then be controlled by high-latitude convection. Further experiments are clearly needed to identify the source region of the patches. Also, future experiments are needed to investigate the relation of the polar cap patches to F-region ionization enhancements observed near the nightside auroral zone with the Chatanika radar.[27]

Time evolution of the patch leads to a steepening of the trailing edge and to the generation or possible restructuring of ionospheric irregularities. A distinct asymmetry is noted in irregularity intensity on the leading and trailing edges. The patch geometry and drift direction suggests that this asymmetry could be a result of the E x B instability.

The ionosonde measurements provide an approximate cross-section through the polar cap F-region patches along the axis of this motion. Bulk velocity and instantaneous Doppler measurements show a velocity of 600—750 m sec^{-1}, in good agreement with the optical measurements. The patches with peak density of 10^6 el cm^{-3} are observed in a weak background ionization ($N_e max \leq 10^5$ el cm^{-3}). The leading edges of these patches have a considerably weaker horizontal N_e gradient than the trailing edges. During the occurrence of these patches under moderately disturbed geomagnetic conditions, no E-region ionization was observed.

---

27. Vickrey, J.F., Rino, C.L., and Potemra, R.A. (1980) Chatanika/TRIAD observations of unstable ionization enhancements in the auroral F-region, Geophys. Res. Lett. 7:789.

References

1. Kelley, M.C., Vickrey, J.F., Carlson, C.W., and Torbert, R. (1982) On the origin and sparial extent of high-latitude F-region irregularities, J. Geophys. Res. 87:4469.
2. Weber, E.J., and Buchau, J. (1981) Polar cap F layer auroras, Geophys. Res. Lett. 8:125.
3. Hardy, D.A. (1983) Intense fluxes of low energy electrons above the auroral oval and in the polar cap, J. Geophys. Res. (in press).
4. Winningham, J.D., and Heikkila, W.J. (1974) Polar cap auroral electron fluxes observed with ISIS I, J. Geophys. Res. 79:949.
5. Lassen, K., and Danielsen, C. (1978) Quiet time pattern of auroral arcs for different directions of the interplanetary magnetic field in the y-z plane, J. Geophys. Res. 83:5277.
6. Gussenhoven, M.S. (1982) Extremely high latitude auroras, J. Geophys. Res. 87:2401.
7. Maezawa, K. (1978) Dependence of geomagnetic activity on solar wind parameters: A statistical approach, Solar Terr. Environ. Res., Japan, 2:103.
8. Aarons, J., Mullen, J.P., Whitney, H.E., Johnson, A.L., and Weber, E.J. (1981) UHF scintillation over polar latitudes, Geophys. Res. Lett. 8:277.
9. Weber, E.J., Buchau, J., Eather, R.H., and Lloyd, J.W.F. (1977) Large scale optical mapping of the ionosphere, AFGL-TR-77-0236. AD A051122.
10. Heelis, R.A., and Hanson, W.B. (1980) High latitude ion convection in the nighttime F region, J. Geophys. Res. 85:1995.
11. Heppner, J.P. (1972) Electric field variations during substorms: OGO 6 measurements, Planet. Space Sci. 20:1475.
12. Bibl, K., and Reinisch, B.W. (1978) The universal digital ionosonde, Radio Sci. 13:519.
13. Buchau, J., Reinisch, B.W., Weber, E.J., and Moore, J.G. (1983) Structure and dynamics of the winter polar cap F region, Radio Sci. (in press).

14. Patenaude, J., Bibl, K., and Reinisch, B. W. (1973) Direct digital graphics, American Lab. 15:95.

15. Tinsley, B.A., Christensen, A.B., Bittencourt, J.A., Angreji, P.D., and Takahashi, H. (1973) Excitation of oxygen permitted line emissions in the tropical nightglow, J. Geophys. Res. 78:1174.

16. Winningham, J.D., and Gurgiolo, C. (1982) DE-2 photoelectron measurements consistent with a large scale parallel electric field over the polar cap, Geophys. Res. Lett. 9:977.

17. Strickland, D.J., Book, D.L. Coffey, T.P., and Fedder, J.A. (1976) Transport equation techniques for the deposition of auroral electrons, J. Geophys. Res. 81:2755.

18. Reinisch, B.W., and Huang Xueqin (1983) Automatic calculation of electron density profiles from digital ionograms, 3. Processing of bottomside ionograms, Radio Sci. 18:3.

19. Weber, E.J., Brinton, H.C., Buchau, J., and Moore, J.G. (1982) Coordinated airborne and satellite measurements of equatorial plasma depletions, J. Geophys. Res. 87:10503.

20. Rino, C.L. (1982) On the application of phase screen models to interpretation of ionospheric scintillation data, Radio Sci. 17:855.

21. Rino, C.L., and Livingston, R.C. (1982) On the analysis and interpretation of spaced receiver measurements of transionospheric radio waves, Radio Sci. 17:845.

22. Livingston, R.C., Rino, C.L., McClure, J.P., and Hanson, W.D. (1981) Spectral characteristics of medium-scale equatorial F region irregularities, J. Geophys. Res. 86:2421.

23. Linson, L.M., and Workman, J.B. (1970) Formation of striations in ionospheric plasma clouds, J. Geophys. Res. 75:3211.

24. Heelis, R.A., Lowell, J.A., and Spiro, R.W. (1982) A model of the high-latitude ionospheric convection pattern, J. Geophys. Res. 87:6339.

25. Roble, R.G., Dickinson, R.E., and Ridley, E.C. (1982) Global circulation and temperature structure of thermosphere with high latitude plasma convection, J. Geophys. Res. 87:1559.

26. Knudsen, W.C. (1974) Magnetospheric convection and the high latitude F_2 ionosphere, J. Geophys. Res. 79:1046.

27. Vickrey, J.F., Rino, C.L., and Potemra, R.A. (1980) Chatanika/TRIAD observations of unstable ionization enhancements in the auroral F-region, Geophys. Res. Lett. 7:789.